Perturbed angular-correlation experiments on ^{111}In in oxidized fcc metals and their oxides

W. Bolse, M. Uhrmacher, and K. P. Lieb

II. Physikalisches Institut der Universität Göttingen, D-3400 Göttingen, Federal Republic of Germany

The perturbed angular correlation (PAC) method has been employed to study the hyperfine interaction of the 245-keV state in ^{111}Cd, following ^{111}In implantation into the fcc metals Ag, Al, Cu, Ni, Pd, Au, and Pt and subsequent oxidation. Broad quadrupole frequency distributions around a peak frequency $\langle \omega_1 \rangle = 160$ MHz were found in all systems and attributed to oxygen trapping at ^{111}In. The fraction of oxidized ^{111}In increases with the oxidation temperature in such a way that about 50% of the implanted In ions have trapped oxygen at 60% of the melting temperature of the host. An interpretation of these frequency distributions has been attempted on the basis of PAC measurements for ^{111}In implanted into the metal oxides AgO, Ag$_2$O, and In$_2$O$_3$. In these systems, well-defined electric field gradients have been found which can be related to the respective crystallographic structures. In addition, the magnetic hyperfine interaction of ^{111}In in antiferromagnetic NiO proves substitutional implantation.

I. INTRODUCTION

In the 1960s, the processes occurring during the oxidation of metals and binary alloys have been studied in much detail, using, for instance, optical and electron-microscopy techniques.[1] The gross features of the oxidation kinetics are well accounted for by Wagner's theory[2] and depend mainly on the concentrations and diffusion constants of the reacting partners.

More recently, Pasquevich *et al.*[3] and Wodniecki and Wodniecka[4] have pioneered the application of the perturbed angular correlation technique (PAC) to the study of the (internal) oxidation process in dilute In *Ag* alloys. This hyperfine method pictures the microsurrounding of radioactive ^{111}In on a subnanometer scale. Roughly speaking, one measures the changes in the electric field gradient (EFG) introduced by the trapping (and release) of oxygen atoms at the site of the ^{111}In probe atom. The high sensitivity of the PAC method to the immediate neighborhood allows one to study the early states of oxidation, oxide precipitation, and the effect of thermally- or radiation-induced defects, as discussed in detail by Bolse *et al.*[5] and by Schröder *et al.*[6]

In this paper we report on the extension of these previous PAC measurements to dilute binary alloys with other fcc metals, including the other noble metals Pd, Pt, and Au, as well as the less noble metals Al, Ni, and Cu. One of the motivations of these experiments was to clarify to what extent the PAC method is suitable for the study of the oxidation kinetics and for the differentiation between various types of oxidation processes (internal or external oxidation of ^{111}In, bulk oxidation). More specifically, we also wanted to see whether the observed EFG arises mainly from the In—O bond length or from the lattice in which In-O is embedded.

A second set of PAC experiments deals with the hyperfine interaction of ^{111}In implanted into metal oxides, such as AgO, Ag$_2$O, In$_2$O$_3$. The binding in these oxides is mainly ionic; therefore the observed EFG parameters can be directly related, via simple point-charge model, to the crystallographic structures of the oxides. The results of these experiments were essential to calibrate the magnitude of the EFG and thus understand the more complex situations prevailing in the oxidized binary alloys. Some preliminary results of this survey have been previously communicated.[7,8]

II. PAC METHOD

The perturbed-angular-correlation (PAC) method is highly sensitive to the microsurrounding of the probing atom, as the electric field gradient (EFG) scales inversely with the third power of the distances between the EFG-generating charges and the probe atom. As a perfect cubic lattice provides no EFG to a substitutional probe atom, many experiments were performed in fcc metals to elucidate the nature of point defects trapped to the probe atom.[9–11] The PAC method can also be applied to more complex situations where different species (vacancies, other atoms) are trapped at the probe atom. As the method has already been explained extensively (see, e.g., Ref. 12), the following section will describe the experimental setup and the strategy employed to analyze the data. In particular, the case of a damped perturbation function will be discussed, as it became an important part in the analysis of the experiments described later on.

A. PAC apparatus

The PAC measurements were carried out in a coplanar setup of four 2 in.$\times$2 in. NaI(Tl) detectors arranged at $\theta_D = 90°$. The time resolution was 3.5 ns [full width at half maximum (FWHM)] in the dynamic range between 140- and 280-keV γ-ray energy. In some experiments these NaI detectors were replaced by four $1\frac{3}{4}$ in.$\times 1\frac{1}{2}$-in. BaF$_2$ detectors[13] to make use of their better time resolution of 0.7 ns (FWHM). The detectors were connected to a conventional slow-fast coincidence circuit as described

in Ref. 14 to allow for high counting rates. Twelve time spectra $N(t,\theta)$ of 1024-channel resolution of all possible start-stop combinations of the four detectors were measured simultaneously, routed, and stored in a 16×1024-channel 24-bit deep histogramming CAMAC (computer-aided measurement and control) memory. In this way the data-collection time was drastically reduced without loss of statistics.

Eight of the twelve time spectra refer to a correlation angle $\theta = 90°$ and four to $\theta = 180°$. After subtraction of a linear background and calculating the geometric average of equivalent spectra, the experimental perturbation function $R(t)$ was calculated as

$$R(t) = 2 \frac{N(t, \theta = 180°) - N(t, \theta = 90°)}{N(t, \theta = 180°) + 2N(t, \theta = 90°)} = A_2^{\text{eff}} G_2(t) . \quad (1)$$

The effective anisotropy coefficient A_2^{eff} was measured separately with a fully annealed α-particle-irradiated Ag sample, showing an unperturbed angular correlation $[G_2(t) = 1]$.

B. The perturbation function $G_2(t)$

The EFG is characterized by a tensor of rank 2. After the diagonalization and ordering of the diagonal elements as $|V_{zz}| \geq |V_{yy}| \geq |V_{xx}|$, the asymmetry parameter $\eta = (V_{xx} - V_{yy})/V_{zz}$ $(0 \leq \eta \leq 1)$ is introduced. The two parameters V_{zz} and η are sufficient to describe an EFG. The hyperfine interaction of the quadrupole moment Q of the isomeric state in ^{111}Cd(245 keV, $\frac{5}{2}^+$) with an EFG results in the hyperfine splitting of the $\frac{5}{2}$ level into three sublevels. The transition energies between these levels are proportional to the quadrupole frequency

$$\omega_Q = eQV_{zz}/[4I(2I-1)\hbar] .$$

Usually, the quadrupole coupling constant ν_Q, which is independent of the nuclear spin I, is defined as

$$\nu_Q = eQV_{zz}/h = 4I(2I+1)\omega_Q/2\pi$$
$$= 20\omega_Q/\pi \quad (\text{for } ^{111}\text{Cd}) . \quad (2)$$

If the EFG is not axially symmetric $(\eta > 0)$, then the energies of the different hyperfine levels can be calculated numerically[15] and in the case of a static EFG the perturbation function $G_2(t)$ is written as

$$G_2(t) = \sum_{n=0}^{3} S_{2n}(\eta)\cos[\omega_n(\eta, \nu_Q)t] . \quad (3)$$

The periodic patterns which are observed in the experimental $R(t)$ function are caused by the transition frequencies $\omega_n = g_n(\eta)\nu_Q$. The amplitudes S_{2n} and the functions $g_n(\eta)$ can be calculated according to Ref. 15. Therefore, the Fourier-transformed experimental $R(t)$ function exhibits a triple of ω_n values (except for $\eta = 1$) which allow a unique determination of the coupling constant ν_Q and the asymmetry parameter η.

C. Damping of the $G_2(t)$ function

Experimental PAC spectra in more complex situations show, in addition to the expected modulation of the angu-

lar correlation, a damping of the amplitudes of the oscillations. In particular, the trapping of oxygen at ^{111}In sites normally leads to a strong damping, as will be demonstrated in Sec. IV. Therefore some phenomena which may cause a damped $R(t)$ function will now be discussed in more detail.

1. Finite time resolution

The first type of damping is introduced by the finite time resolution of the PAC apparatus. An amplitude factor $A_n(\omega_n) = S_{2n}^{\text{eff}}/S_{2n} \leq 1$ can be calculated[16] for different time resolutions and is introduced in Eq. (3). For a NaI setup with the typical time resolution of 3.5 ns, A_n decreases from $A_n(500 \text{ MHz}) = 0.77$ to $A_n(750 \text{ MHz}) = 0.54$, whereas for the BaF$_2$ setup the A_n are close to unity: $A_n(750 \text{ MHz}) = 0.98$. If an EFG $(\eta = 0)$ is observed which is characterized by $\omega_1 = 150$ MHz, then the third transition frequency $\omega_3 = 450$ MHz is clearly affected by the time resolution of a NaI setup. The oscillation pattern broadens and η is difficult to determine. Nevertheless, this type of damping can be overcome by fast detectors.

2. Fluctuating EFG's

A second damping mechanism will be observed if the EFG itself is not constant during the lifetime of the nuclear state. The reason could be a fast-diffusion process which changes the microsurrounding of the probe as observed in ^{181}TaHf.[17] More often, the "aftereffects" are considered a source of quickly fluctuating EFG's.[18] As ^{111}In decays via electron capture to the excited states of ^{111}Cd, one may expect a delayed refilling of the ^{111}Cd electron shells in systems with a low density of free electrons. Applying the theory of Abragam and Pound,[19] the observed anisotropy of the angular correlation decays exponentially as $A_2' = A_2^{\text{eff}}\exp(-\lambda_2 t)$. In the case of fluctuating EFG's the perturbation function will approach $G_2(t \to \infty) = 0$, whereas in the static case $G_2(t)$ reaches the so-called "hard-core value" $G_2(t \to \infty) = S_{20}$. Thereby the static and the dynamic case can be distinguished experimentally.

3. EFG Distributions

In most cases the damping arises from a mixture of similar EFG's which are caused by small irregularities of the atomic positions in the next neighborhood of the probe atom. The perturbation function $G_2(t)$ has to be folded with the distribution function $P(\nu_Q)$ of the interaction frequencies,

$$G_2(t) \Longrightarrow \int_{-\infty}^{+\infty} P(\nu_Q)G_2(t)d\nu_Q . \quad (4)$$

The real EFG distribution is usually approximated by a Lorentzian (LD) or Gaussian distribution (GD), and the perturbation function is written as

$$G_2(t) = \sum_{n=0}^{3} S_{2n}(\eta)\cos[g_n(\eta)\langle \nu_Q \rangle t]$$

$$\times \exp[-g_n(\eta)\delta\nu_Q t] \quad (\text{LD}) , \quad (5a)$$

$$G_2(t) = \sum_{n=0}^{3} S_{2n}(\eta)\cos[g_n(\eta)\langle\nu_Q\rangle t]$$

$$\times \exp[-(g_n(\eta)\delta\nu_Q t)^2] \quad \text{(GD)} . \qquad (5b)$$

These approximations have a critical simplification. In the folding procedure, one assumes a distribution of the ν_Q values, but uses a *fixed* η *parameter*. Forker[20] investigated the influence of EFG distributions on the determination of η.

Figure 1 shows an increasing deviation of the fitted η^{fit} from that of the well-defined EFG if the distribution width increases. Figure 2 gives an example: The probe is placed into a perfect crystal and the PAC parameters are $\nu_Q = 128$ MHz, $\eta = 0$, and $\delta\nu_Q/\nu_Q = 0$. If one assumes a distribution of the EFG characterized by $\delta\nu_Q/\nu_Q = 50\%$, the fit yields $\eta^{\text{fit}} = 0.5$, as extrapolated from Fig. 1. An increasing η value causes an increase of $g_1(\eta)$ and, as a consequence of $\omega_n = g_n(\eta)\nu_Q$, a smaller quadrupole coupling constant $\langle\nu_Q\rangle^{\text{fit}} = 95$ MHz. Figure 2 also demonstrates that the Fourier analysis may help to solve this problem, as the maximum of ω_1 for the well-defined EFG and for the broad distribution coincide. But it is evident that the analysis of distributed EFG's needs confirmation by well-defined complexes.

D. Classification of the PAC parameters

The experimental perturbation function $R(t)$ is fitted with a theoretical $G_2(t)$ function (5) using the CERN fitting routine MINUIT.[21] The program handles a maximum of five different sites and the perturbation function is written as

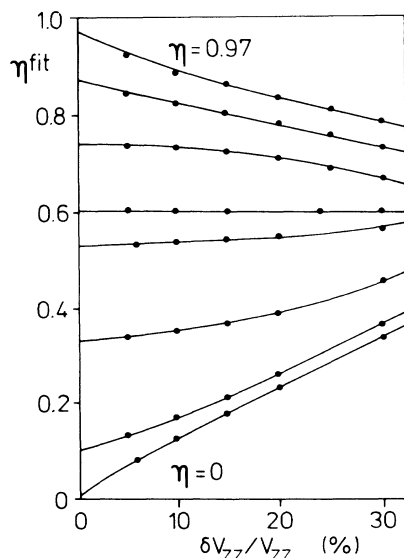$$R(t) = A_2^{\text{eff}} \sum_{i=1}^{5} f_i G_2^i(t), \quad \sum f_i = 1 . \qquad (6)$$

FIG. 1. Variation of the fitted values η^{fit} on the width parameter $\delta V_{zz}/V_{zz}$ for increasing η values. (Redrawn from Ref. 20).
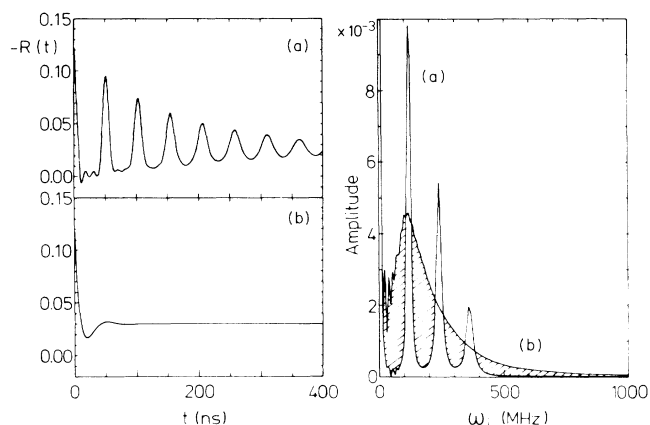
FIG. 2. Perturbation functions with (a) little damping and (b) large damping and resulting Fourier spectra. Note that the maximum $\langle\omega_1\rangle$ of the broad frequency distribution coincides with the lowest component ω_1 of the weakly damped perturbation function.

Each site is characterized by its fraction f_i, which describes the site occupation, and by the structural parameters ν_{Q_i}, η_i, and $\delta\nu_{Q_i}$: ν_{Q_i} and η_i are the "fingerprints" of the EFG at site i and contains information about the homogeneity of this site. In this way the PAC experiments yield information about the oxidation dynamics, as well as about the geometry of the objects built during the oxidation process.

III. EXPERIMENTAL DETAILS

A. [111]In implantation

The PAC probe [111]In$^+$ was implanted with an energy of 500 keV into all metals and oxides (except AgO and Ag$_2$O) with the help of the Göttingen 500-kV ion implanter IONAS,[22] which is equipped with a hollow-cathode ion source.[23] When optimizing the transmission of the radioactive [111]In$^+$ beam through the implanter, a procedure was developed which usually gives a transmission of 10%, but may also reach 25%.

Carrier-free ^{111}In is commercially available as InCl$_3$ in 0.04 mol HCl. Microliter droplets are put at the tip of a small steel rod where they are dried by ir heating. This active region is then covered by a small steel tube and positioned just 3 mm inside the entrance of the high-temperature oven of the ion source. The cylindrical shape of the InCl$_3$ container prevents the possibility of ^{111}In being trapped at colder parts of the oven. Before the source is started with the working gas Ar, the accelerating voltage is applied and the focusing elements are tuned. The indirect heating by the hot filament is sufficient to dissociate and evaporate [111]InCl$_3$. For 5–10 min a mass-111 beam of up to 7 nA is observed, sufficient to produce a target with 3.7 MBq activity. Due to the high ^{111}In transmission, implantations can be carried out in intervals of 40 min.

TABLE I. Metal foils used, implantation ranges, and widths of 500-keV ^{111}In$^+$ ions.

Sample	Thickness (μm)	Purity (%)	Range (nm)	FWHM (nm)
Ag	100	99.999	68	81
Al	50	99.999	190	120
Au	50	99.999	45	75
Cu	25	99.999	71	63
Ni	50	99.998	67	58
Pd	100	99.997	40	66
Pt	25	99.999	60	70

B. Target preparation

The thickness and purity of the metallic targets used are given in Table I. The foils were cut to a size of 5×10 mm^2 without special annealing or surface treatment. Also given are the projected ranges and the widths of the Gaussian implantation profiles for 500-keV ^{111}In$^+$ ions as calculated with the code DIMUS.[24]

The preparation of the oxide targets was more complicated, as AgO and Ag$_2$O were obtained as fine powders. The silver oxides were irradiated in the cyclotron to take advantage of the deep-penetration possibilities of 36-MeV α particles. Pressed powder ($\sim$100 mg/cm^2) was packed in 50-μm Al foils. The energy loss of the α beam in this Al foil is only 2 MeV and ^{111}In is produced via the ^{109}Ag ($\alpha, 2n$) nuclear reaction within the target with a sufficiently high cross section.

This method cannot work during the 500-keV implantation of ^{111}In into silver and indium oxides, as the range of these ^{111}In$^+$ ions in Al is only 0.14 μm. Therefore the pressed oxides were covered with Al foils too, but a (5×5)-mm^2 window was left open for the ^{111}In implantation. A sintering procedure was not possible because of the weak thermal stability of the oxides; nevertheless, the implantation process caused no observable damage by heating up the targets. After the implantation they were covered by 50-μm Al foils prior to further thermal treatments.

NiO targets were obtained by heating 50-μm Ni foils at $T_{ox} = 1223$ K in a 200-mbar O$_2$ atmosphere. After this treatment the surface showed a stable dark-brown layer. A Rutherford-back-scattering (RBS) experiment with 1-MeV α particles was performed with IONAS and confirmed a stoichiometric NiO layer exceeding a thickness of 0.5 μm.

A film of In$_2$O$_3$ on an Al backing was prepared by Ovadyahu[25] by evaporating In$_2$O$_3$ mixed with 10 at. % In metal with an electron gun in an oxygen atmosphere of 5×10^{-4} mbar. Details of the method are given in Ref. 25. The thickness of this layer was determined in a RBS experiment to be 0.36 μm.

C. Thermal treatments

After implanting ^{111}In into the fcc metals, radiation damage typically governs the $R(t)$ function. In a first step, this damage was annealed in vacuum (10^{-6} mbar) before any oxidation treatment was started. The max-

imum annealing temperature was 1223 K. A movable holder allowed placement of the sample into the hot oven. The typical heating-up time was thus reduced to about 3 min, the corresponding cooling-down time about 10 min. Annealing of radiation damages in metals was done for 60 min.

The oxidation of the metal samples took place in a quartz tube heated by an electrical oven. First, the tube was filled several times with oxygen and then adjusted to a pressure of 200 mbar. The sample was placed on a movable holder and shifted into the hot region of the tube. The uncertainty in oxidation temperature was ± 5 K and the heating-up or cooling-down times are similar to those obtained in the vacuum oven. During the isochronal oxidations (see Sec. IV) the samples were kept at each temperature for 15 min.

The metal oxide samples also passed an isochronal annealing cycle after ^{111}In implantation. They were kept under vacuum at the given temperatures for 15 min, while the perturbation functions were measured at room temperature. In this way phase transitions between oxides with different oxygen contents were observed, e.g., AgO$\rightarrow$Ag$_2$O. The thermal stability of AgO, Ag$_2$O, and NiO did not allow preceding annealing of the radiation damages, but it was assumed that such damage is repaired during the first phase transition.

IV. RESULTS

A. Oxidation of ^{111}In in fcc metals

After implantation and vacuum annealing of about 10^{12} radioctive ^{111}In atoms in the fcc metals Ag, Al, Au, Cu, Ni, Pd, and Pt, fully unperturbed PAC spectra were obtained (except in the case of Pd), indicating substitutional positions of the ^{111}In within the lattice. The oxidation of ^{111}In in each sample was then observed during a cumulative isochronal oxidation cycle. After each oxidation step, a PAC spectrum was taken at $T_m = 295$ K (for Ni at $T_m = 700$ K). Up to a critical oxidation temperature, the spectra remained unperturbed (except for further annealing of Pd). At higher T_{ox} values, an increasing fraction f_2 evolves, characterized by a broad frequency distribution ($\delta\nu_{Q_2}/\nu_{Q_2} \geq 30\%$). As an example, Fig. 3 shows $R(t)$ spectra measured in the Pd host; the corresponding figure for ^{111}In in Ag can be found in Ref. 7.

The dependence of this fraction f_2 on the oxidation temperature T_{ox} reflects the oxidation kinetics, as illustrated in Fig. 4. With the exception of Al, all metals show a similar behavior: f_2 rises up to 100% for low-melting-point metals and reaches $f_2 \geq 60\%$ in the case of Pt and Pd, due to the limited temperature range of our oven ($T_{ox} \leq 1223$ K). It thus can be inferred that all ^{111}In probe atoms finally have trapped oxygen, as was demonstrated in the early studies of internal oxidation of In in Ag.[3,4] Especially in the case of Ag it was shown that this process of oxygen trapping is diffusion controlled.[26]

If one determines the temperature $T_{50\%}$, at which half the initially unoxidized ^{111}In atoms have trapped oxygen, a strong correlation with the melting temperatures of the host is evident (Fig. 5): the oxidation starts at

$T_{ox} \approx 0.6 T_{melt}$, where the thermal production of vacancies, necessary for substitutional diffusion, sets in. We take this as a hint that the oxidation is not only controlled by the fast interstitial diffusion of oxygen, but also by substitutionally diffusing indium. As will be discussed later the observed hyperfine parameters for oxidized ^{111}In in the fcc metals suggest the formation of very small In_2O_3 precipitates. Such a process requires In diffusion.

As the Al and Cu samples are in contact with air, their surfaces are covered with oxide layers. Since we did no surface treatment, these samples show, already after vacuum annealing, some perturbed fraction f_2 [Cu-1 in Fig. 4(b)] which probably is correlated to this oxide layer. One Cu sample was polished before ^{111}In implantation and indeed no perturbed fraction was observed after vacuum annealing[27] [Cu-2 in Fig. 4(b)]. A more detailed investigation for the system In Al is being carried out at present

to test this point.[28]

The fitted hyperfine parameters $\langle v_{Q_2} \rangle$, $\langle \eta_2 \rangle$, and $\delta v_{Q_2}/\langle v_{Q_2} \rangle$ are given in Table II. For Ag, Al, Au, Pt, Pd, and Ni the measured $\langle v_{Q_2} \rangle$ values were found to be independent of T_{ox}, whereas Cu showed a continuous decrease of $\langle v_{Q_2} \rangle$ during the oxidation. The $\langle v_{Q_2} \rangle$ values obtained for Au are constant within one sample but scatter for different samples around the value reported in Ref. 29. To demonstrate the similarity of the PAC spectra obtained after the oxidation treatment, all spectra with the maximum amount of f_2 are compared with each other in Fig. 6.

The fraction $f_1 = f - f_2$, characterized by $v_Q = 0$, is attributed to ^{111}In on substitutional defect-free sites. This

FIG. 3. Perturbation functions $R(t)$ for ^{111}In in Pd after partial annealing at $T_a = 1175$ K, after oxidation at $T_{ox} = 1075$ K and after oxidation at $T_{ox} = 1175$ K.
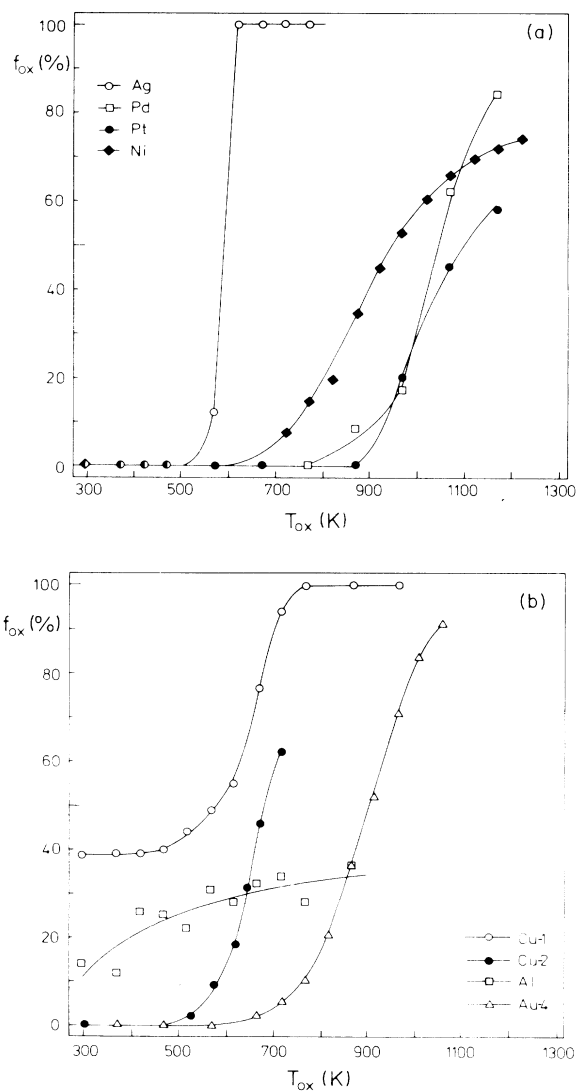

FIG. 4. Oxidized fractions of ^{111}In in fcc metals observed in cumulative isochronal oxidation cycles: (a) hosts Ag, Pd, Pt, and Ni; (b) hosts Cu, Al, and Au. For Cu and Au the results for different samples are displayed.

TABLE II. Hyperfine parameters of oxidized ^{111}In in fcc metals (fraction 2).

Host	$\langle \nu_{Q_2} \rangle$ (MHz)	η_2	$\delta\nu_{Q_2}/\nu_{Q_2}$ (%)	$\langle \omega_1 \rangle$ (MHz)
Ag	84(5)	0.49(10)	50	96(5)
	119(8)	0.70(12)	40[a]	158(8)
Al	108(7)	0.62(10)	45	135(7)
Au-3[d]	92(5)	0.85(10)	42	137(5)
Au-1[d]	137(7)	0.55(10)	42	163(7)
Au-4[d]	170(10)	0.50(10)	28	194(10)
Au	143	0.55	35[b]	170
Cu	210–102	0.4–0.6	50	223–128
Ni	136(5)	0.83(10)	35[a]	200(5)
Pd	130(7)	0.59(10)	50	160(7)
Pt	128(7)	0.68(10)	27	168(7)

[a]$T_{ox} \geq 700$ K.
[b]Reference 29.
[c]$T_m = 700$ K.
[d]Numbers indicate different samples.

assumption can be directly proven for the ferromagnetic Ni host, as below the Curie temperature f_1 should show pure magnetic hyperfine interaction and the known temperature dependence of the Larmor frequency ω_L.[30] In the case of Ni, perturbation functions were therefore measured after each oxidation step at room temperature (RT) and above the Curie temperature. The fraction $f_{1 \, mag}$ (RT) was found to be equal to f_1 ($T_m = 700$ K), as was the oxidized fraction f_2 obtained at both measuring temperatures. A second experiment was conducted to check the temperature dependence of the Larmor frequency $\omega_L(T)$ of this fraction $f_{1 \, mag}$. The sample was partially
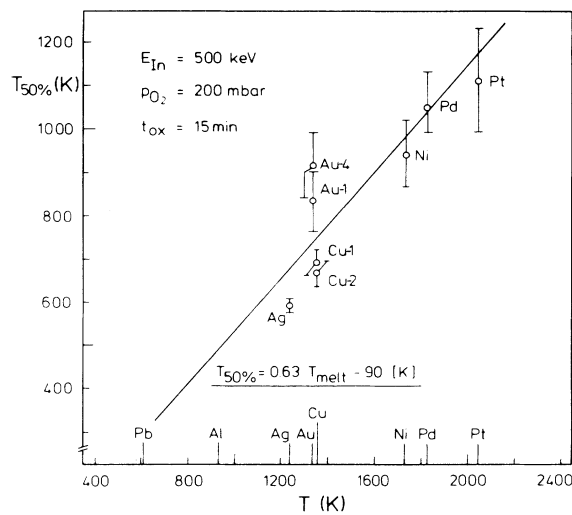
oxidized ($f_{1 \, mag} = 48\%$ at $T_{ox} = 973$ K) and the measuring temperature T_m was varied in the range $T_m = 295$–700 K. The corresponding perturbation functions are given in Fig. 7. The Larmor frequency follows a modified Curie-Weiss law $\omega_L(T_m)/\omega_L(0) = (1 - T_m/T_c)^\beta$ with the parameters $T_c = 631$ K, $\omega_L(0) = 119(2)$ MHz, and $\beta = 0.380(5)$, in perfect agreement with the work by Hohenemser and collaborators.[30] This fact proves that the fraction f_1 does, in fact, correspond to ^{111}In on substitutional sites in the ferromagnetic Ni lattice. The oxidized fraction f_2 seen as quadrupole interaction between trapped oxygen and ^{111}In is clearly observed at $T_m = 623$ K and above the Curie point (Fig. 7).

FIG. 5. Correlation of the temperature $T_{50\%}$, at which 50% of the ^{111}In atoms are oxidized, and the melting temperatures T_{melt}.
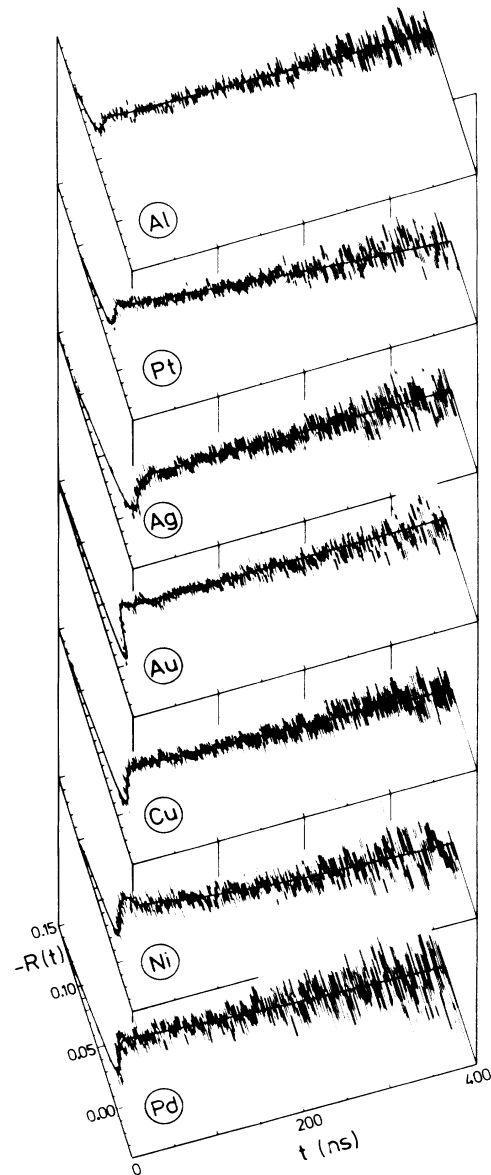

FIG. 6. Comparison of perturbation functions for ^{111}In in fcc metals obtained with maximum oxidized fraction.

TABLE III. Hyperfine parameters observed after ^{111}In implantation into AgO and Ag_2O.

Irrad. oxide	f_i	v_{Q_i} (MHz)	η	δv_{Q_i} (MHz)	ω_1 (MHz)	T_a (K)
AgO	1	200–300	0.1–0.4	80–100	213–286	as-irr.
	2	323(5)	0.0(1)	6	300(5)	as-irr.
	3	105–120	0.0–0.4	40–60	112(5)	420–620
	4	129(4)	0.00(5)	4	120(4)	420–620
	5	95–110	0.7(1)	45	126–146	> 620
	6	0	0	0	0	> 720
Ag_2O	3	90–110	0.4–0.5	40–50	96–125	as-irr.
	5	110(10)	0.6–0.7	50	138–146	> 670
	6	0	0	0	0	> 720

B. [111]In in the oxides of the fcc metals

The broad frequency distributions summarized in Table II remind us of the difficulties in determining the structure of the [111]InO_x complexes (see Sec. II C 3). The experiments discussed in this section were an attempt to study the EFG of ^{111}In in metal oxides hoping that one may find the same microsurroundings as seen after In oxidation in the metal host. The metal oxides are usually thermally unstable during vacuum annealing and transform into oxides with smaller oxygen content.

1. The silver oxides AgO and Ag_2O

The silver oxide with the highest oxygen content, AgO, has a monocline lattice structure[31] (space group $P2_1/c$, $a = 5.852$ Å, $b = 3.478$ Å, $c = 5.459$ Å, $\beta = 107° 30'$). As depicted in Fig. 8, the Ag ions form a fcc sublattice, while 50% of the tetrahedral places are occupied by oxygen. This results in two nonequivalent sites for Ag, one (Ag^+) with a collinear coordination of two O^{2-} ions and the other (Ag^{3+}) with a nearly planar quadratic configuration of four O^{2-} ions. The two different charge states of Ag^+ and Ag^{3+} were suggested in neutron-scattering experiments, whereas x-ray analysis showed only Ag atoms surrounded by four oxygen atoms, as displayed in Fig. 8.[31] Our experiments propose only one site occupied by [111]In (see below), and without making a final decision on the structure we assume that [111]In^{3+} prefers the site of Ag^{3+}

The other silver oxide, Ag_2O, crystallizes in the highly symmetric space group $Pn3$ (cuprit). The Ag ions form a cubic fcc sublattice ($a = 4.72$ Å) and 25% of the tetrahedral sites in the direction of the space diagonal are occupied by oxygen:[31] each Ag^+ ion has a collinear coor-
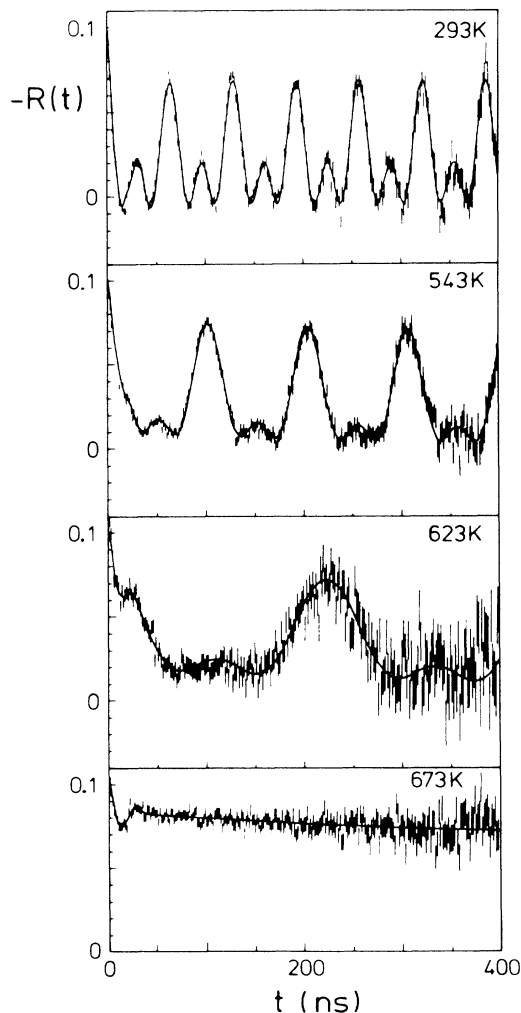

FIG. 7. PAC spectra of ^{111}In in a partially oxidized Ni sample ($f_2 = 48\%$), taken at the measuring temperatures indicated.
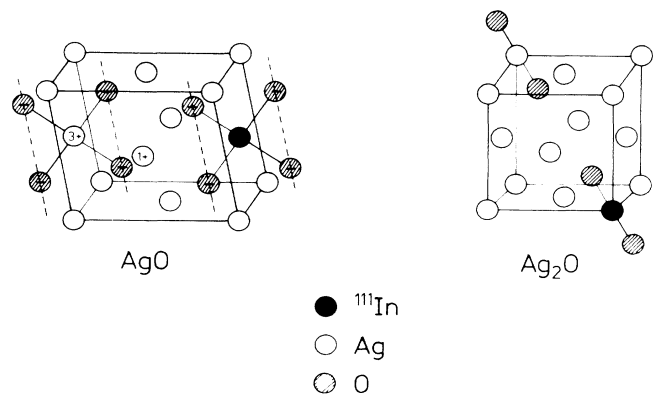

FIG. 8. Oxygen coordinations in AgO and Ag_2O.

dination by two O^{2-} ions as shown in Fig. 8.

[111]In was introduced into the silver oxides by means of the reaction [109]Ag$(\alpha,2n)$ using the 36-MeV α beam of the Göttingen cyclotron. The result of a vacuum annealing of α-irradiated AgO is shown in Fig. 9. Six fractions were identified. Their PAC parameters are summarized in Table III and their dependence on the annealing temperature T_a is displayed in Fig. 10.

After irradiation, only the two fractions labeled f_1 and f_2 are observed. The asymmetry parameter η_2 was determined by means of a setup of BaF_2 detectors. The corresponding Fourier spectrum is given in Fig. 11. It clearly illustrates that the maximum of the broad frequency dis-
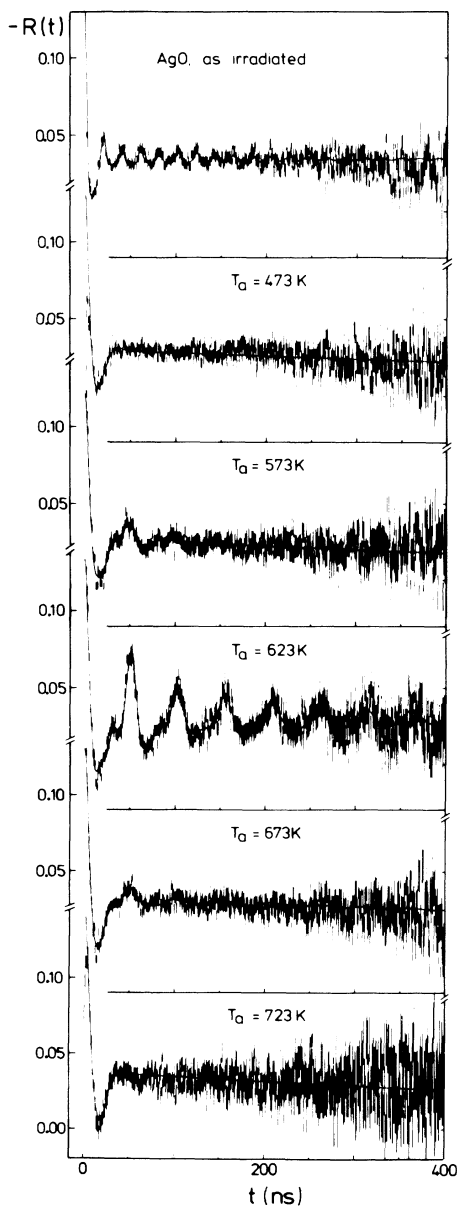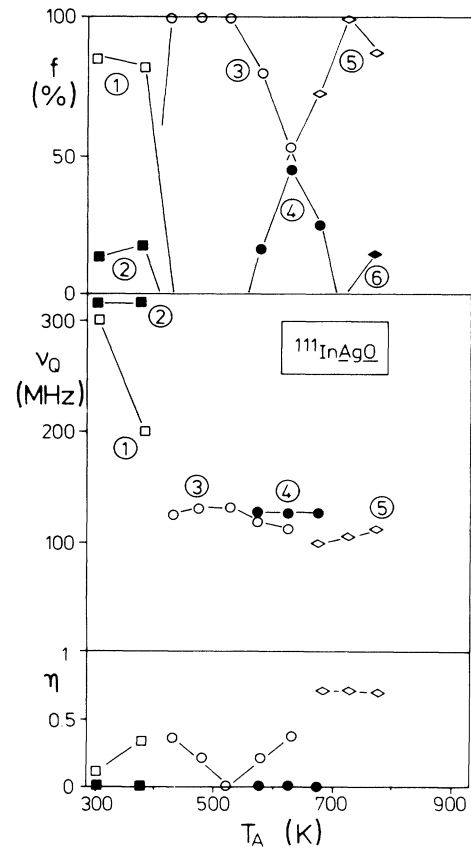
FIG. 10. Fractions f_1, quadrupole frequencies v_{Q_1}, and asymmetry parameters η_1 of complexes observed in the system [111]In AgO.

tribution of f_1 coincides with the ground frequency ω_1 of the well-defined EFG of fraction f_2. We conclude that below 400 K all ^{111}In atoms sense a similar EFG, but that a large fraction is affected by more distant lattice imperfections, possibly due to the irradiation process. In the temperature range $423 \le T_a \le 623$ K, a new combination

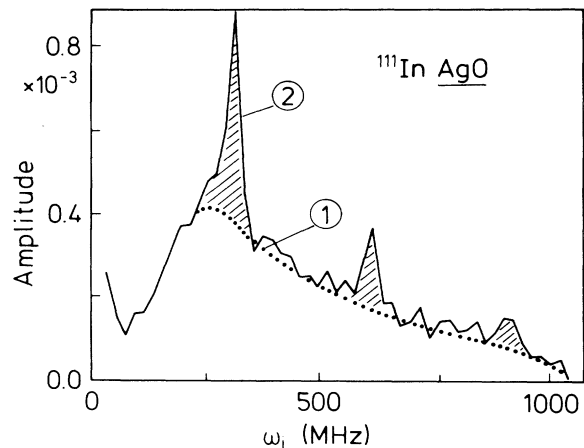FIG. 9. Perturbation functions taken in an isochronal annealing cycle after α irradiation of AgO.

FIG. 11. Fourier spectra of complexes 1 and 2 in the system [111]In AgO, obtained with BaF_2 detectors.

of a broad distribution and a well-defined frequency is observed (f_3, f_4). At $T_a > 623$ K, these fractions disappear again and now a broad frequency distribution f_5 appears which is known from oxygen trapping to ^{111}In in preoxidized Ag.[3,4] At still higher temperatures ^{111}In loses oxygen and does not sense any EFG (cubic site, $v_{Q_6} = 0$).

A similar behavior is observed during vacuum annealing of the Ag_2O samples whch had been irradiated in the cyclotron. Three fractions listed in Table III are sufficient to describe the PAC spectra. Above 773 K, again the increase of the unperturbed fraction f_6 is observed, whereas the transformation from f_3 to f_5 around 650 K is less pronounced.

As the three temperature regions coincide with the dissociation processes $AgO \rightarrow Ag_2O \rightarrow Ag$,[32] we identify f_2 as substitutional ^{111}In in AgO and f_4 as substitutional ^{111}In in Ag_2O. The fraction f_5 is well known from interstitial oxygen trapping at ^{111}In in silver, while f_6 is the fraction of ^{111}In atoms in an oxygen-free cubic Ag surrounding. The fraction f_3 represents ^{111}In in a Ag_2O lattice, possibly affected by further defects. A similar complex was found after overlapping implantation of oxygen and ^{111}In into Ag.[8,33]

At first sight, it seems disturbing that the fraction f_4 attributed to ^{111}In on substitutional sites in Ag_2O is only seen in the AgO sample. However, during the dissociation of this unstable oxide, the damage from the irradiation anneals and a relatively large fraction of ^{111}In reaches substitutional sites in Ag_2O now formed. In the case ^{111}In Ag_2O the higher annealing temperature needed leads to faster loss of oxygen without a good chance of repairing the Ag_2O lattice.

2. Nickel oxide (NiO)

Nickel oxide has a cubic NaCl structure which consists of a Ni fcc sublattice with eight nearest-neighbor (NN) octahedral oxygen ions around each Ni. For that reason, no EFG for In on substitutional sites is expected. On the other hand, NiO is antiferromagnetic below its Néel temperature $T_N \approx 550$ K, leading to a magnetic hyperfine interaction[34] which can be identified by its temperature dependence.

After implantation, a distribution of EFG's around $\langle v_Q \rangle = 0$ is observed, having a width of $\delta v_Q = 15$ MHz. It is visible as a damping of the Larmor oxcillation in the lower part of Fig. 12. The fitted Larmor frequency $\omega_2(300$ K$) = 242(3)$ MHz is in perfect agreement with that found for a small fraction of 8%, which occurred in the perturbation function after complete oxidation of ^{111}InNi at 1223 K, as shown in the upper part of Fig. 12. This fraction can thus be identified as substitutional ^{111}InNiO. If NiO is annealed above 700 K the oxide decomposes and loses oxygen, as seen also from RBS experiments. The corresponding PAC spectrum shows only a fraction characterized by $\langle v_Q \rangle = 125(10)$ MHz, $\eta = 0.7(1)$, and $\delta v / v_Q = 50\%$.

C. Indium oxide (In$_2$O$_3$)

After the identification of PAC parameters relevant for metal oxides, the other extreme has to be identified also:

the PAC parameters of ^{111}In in its own oxide In_2O_3. The In_2O_3 lattice has space group $Ia3$ and consists of a nearly cubic fcc sublattice for the In^{3+} ions.[35] The O^{2-} ions occupy six out of the eight tetrahedral positions. The empty sites have different positions; therefore; eight cubes of the In sublattice are needed to form the unit cell of In_2O_3. As a consequence, two different In sites exist, each coordinated by six oxygen ions as shown in the inset of Fig. 13. The oxygen coordination is symmetric around a corner atom of the In sublattice (complex "3" of Ref. 36) and less symmetric for the face-centered sites (complex "2b" of Ref. 36). The occupation of the two sites is 1:3.

In a previous PAC experiment with chemically prepared ^{111}InInO_3 powder,[36] we identified, in fact, these two fractions and determined their PAC parameters. The $R(t)$ curves showed a small but observable damping corresponding to $\delta v_Q / v_Q = 12\%$ and 4%, respectively. We now repeated the experiment using a solid In_2O_3 film on Al substrate. The PAC spectra taken at $T_m = 823$ and 300 K revealed the hyperfine parameters:

$$v_{Q_1} = 119(2) \text{ MHz}, \quad \eta_1 = 0.69(5) \quad \text{(complex 2b)},$$

$$v_{Q_2} = 154(2) \text{ MHz}, \quad \eta_2 = 0.00(5) \quad \text{(complex 3)},$$

$$\langle f_2 / f_1 \rangle = 0.30(5).$$

The $R(t)$ data and the deduced Fourier spectrum are given in Fig. 13. Both frequency triplets are well resolved, indicating a nearly undamped PAC spectrum $(\delta v_Q / v_Q < 0.02)$. Therefore both asymmetry parameters could be precisely determined, resulting in $\eta_2 = 0$ as compared to $\eta_2 = 0.32(5)$ in Ref. 36. PAC experiments on the internal oxidation of dilute InAg alloys with In concentrations larger than 10^{-3} at.% (Refs. 4, 26, and 29) showed the occurrence of both In_2O_3 fractions with larger damping in the PAC spectra. Also, the ratio of fractions was normally smaller than 0.33. These PAC data can be
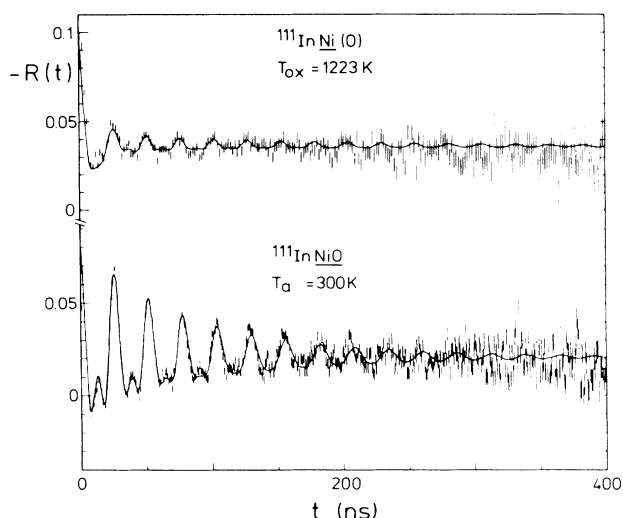

FIG. 12. Perturbation functions for ^{111}In implanted into Ni and oxidized at $T_{ox} = 1223$ K (top) and into NiO (bottom). The data were taken at room temperature. Both spectra exhibit a fraction with Larmor frequency $\omega_L = 242(3)$ MHz.

explained by the formation of In_2O_3 precipitates in Ag. If one assumes small In_2O_3 precipitates surrounded by the host metal that may act as a more distant perturbation for ^{111}In inside the precipitate, the considerations of Sec. II C 3 again apply and we expect broad frequency distributions. In the Fourier spectrum of In_2O_3, both sites have similar main frequencies ($\omega_1 = 160$ and 145 MHz for complexes 2b and 3, respectively). These two frequencies will not be resolved in the Fourier spectra, as soon as the distribution width exceeds $\Delta\omega_1 = 15$ MHz. Therefore a conservative fitting procedure using a minimum of free parameters will always identify the broadly distributed "In_2O_3" PAC spectrum as only one component previously labeled complex "2b." In addition, this complex represents 75% of all ^{111}In in In_2O_3.

As described in Sec. IV A, the oxidation of ^{111}In in fcc metals always results in broad frequency distributions. In Table II the peak frequencies $\omega_1 = g_1(\eta)\nu_Q$ of the distributions in the Fourier spectra are given. Most values agree reasonably well with the ω_1 values of In_2O_3, except that in the Ni and Ag hosts. In addition, the frequency distributions obtained after total disintegration of the oxides NiO, AgO, and Ag_2O are in agreement with each other. We interpret this fact as evidence for the existence of very small In_2O_3 precipitates. Electron microscopy would be
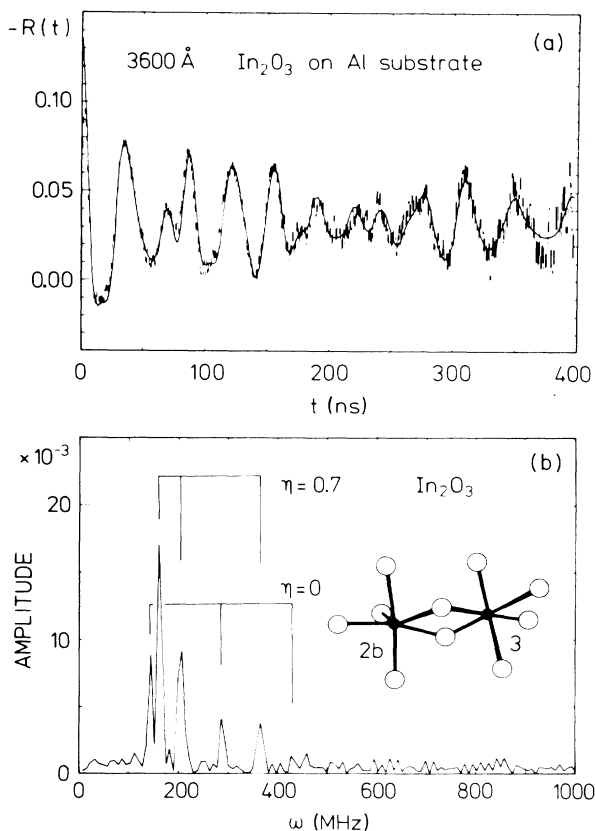
necessary to determine the size of these precipitates and relate them to the PAC spectra.

V. DISCUSSION AND CONCLUSIONS

A. Classification of different oxidation processes

The oxidation of alloys is diffusion controlled.[37,38] The inward diffusion of oxygen occurs, as well as the diffusion of the metal ions to the surface. Figure 14 depicts four extreme situations which may govern the oxidation of ^{111}In-implanted metals. For noble-metal alloys with a low In concentration but high O solubility ($D_{In}/D_O \ll C_O/C_{In}$), the oxidation is controlled by O diffusion into the host metal (internal oxidation) [Fig. 14(a)]. With increasing indium concentration ($C_O/C_{In} \ll D_{In}/D_O$), external oxidation of In at the surface is observed. In this case the outward diffusion of In determines the oxidation process [Fig. 14(b)].

More complicated situations arise in host metals which form their own oxides and for which diffusion in the metal oxide film at the surface is of main importance. This layer can either grow by diffusion of bulk metal atoms to the surface [Fig. 14(c)], or by oxygen diffusion through the oxide layer [Fig. 14(d)]. Several possibilities exist to oxidize In in such a system: Oxygen may diffuse from the metal oxide layer into the metal host and may lead to internal oxidation of In below the metal oxide layer. The inverse case, a growing indium oxide layer on top of the metal oxide, may be found if In diffuses through the oxide to the surface. Within these limits, In can either reach substitutional sites in the metal oxide or diffuse into the

FIG. 13. (a) Perturbation function and (b) its Fourier transform for the system [111]InInO_3. The 360-nm In_2O_3 layer had been deposited onto an Al substrate. The inset illustrates the two oxygen coordinations.
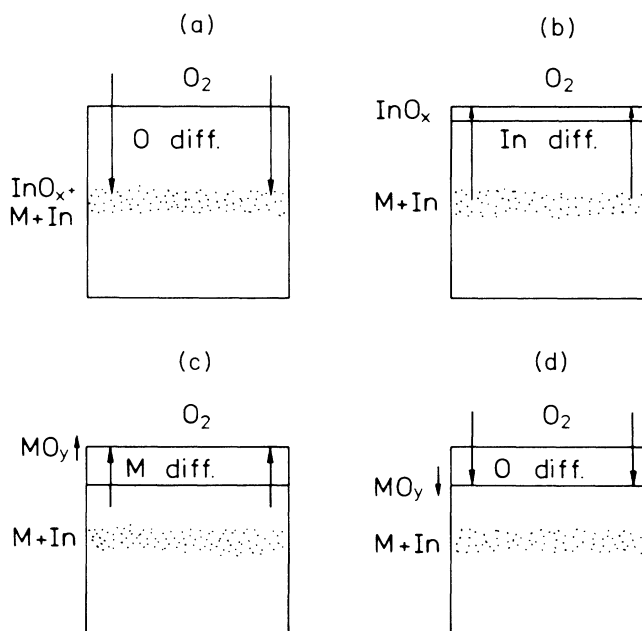

FIG. 14. Oxidation processes discussed in the text: (a) internal oxidation of In; (b) external oxidation of In; (c) and (d) bulk oxidation.

bulk metal without oxidation.

The oxidation mechanism is determined by the change of free energy $\Delta F = \Delta H - T \Delta S$ necessary to form an oxide; oxidation only occurs if ΔF is negative. Figure 15 displays the dependence of F on the oxidation temperature T_{ox} for reactions of the type $M + xO \rightarrow MO_x$. The metals Al, Cu, Ni, and Pd may be oxidized at all temperatures, whereas Ag_2O is only stable below 500 K. Au and Pt are expected to be stable against oxidation. Therefore, pure internal or external oxidation of In without oxidation of the matrix is only possible for the noble metals Au, Pt, and Ag ($T_{ox} \geq 500$ K). These considerations suggest a separate discussion of the less noble metals and the noble metals.

B. [111]In in oxidizable fcc-metal hosts

1. Nickel

Only during the oxidation of Ni were we able to confirm the substitutional site of ^{111}In inside the metal oxide lattice by its magnetic hyperfine interaction. Over 90% of the ^{111}In atoms sense a broad frequency distribution, which we think is typical for small In_2O_3 precipitates.

2. Copper

In Cu the observed frequency is temperature dependent.[7,27] The oxidation of Cu leads to a decreasing total oxygen concentration from the surface to the bulk.[39] The
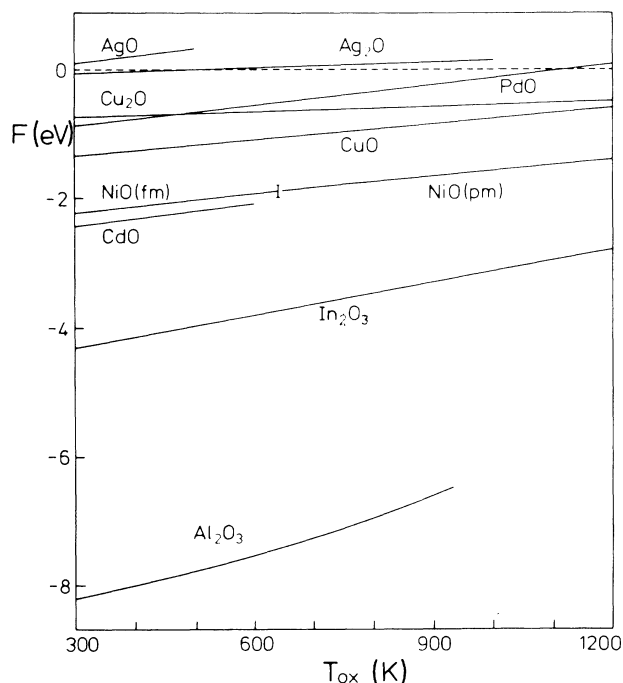

FIG. 15. Free energy F of the reaction $M + xO \rightarrow MO_x$ for the metals studied (Ref. 40). In the case of Ni, oxidation can occur in the ferromagnetic (fm) and paramagnetic (pm) phases.

copper oxides CuO and Cu_2O may be formed and additional oxygen is dissolved in the copper host. The observed dependence of $\langle v_Q \rangle$ on the oxidation temperature may indicate changing fractions of [111]InCu_2O and [111]InCuO during the oxidation cycle. Additional experiments on ^{111}In implanted into the copper oxides are needed to prove this assumption.

3. Aluminum

In the case of Al the oxidation of In is strongly hindered, as seen in Fig. 4. No internal oxidation of In is possible, as the free energy of formation for Al_2O_3 is more negative than that of In_2O_3. However, ^{111}In can be oxidized if solved in Al_2O_3. In fact, recent measurements with InAl alloys[28] show that a small fraction of implanted In diffuses into the Al_2O_3 surface layer, while a larger part diffuses into the bulk material. On the other hand, up to now no reliable PAC measurements of [111]InAl_2O_3 exist. Atkinson[38] proposed that the oxidation of Al below 673 K forms an amorphous oxide layer which would also generate a broadly distributed EFG, in agreement with our data.

C. [111]In in noble fcc-metal hosts

1. Silver

The PAC parameters found for the oxidation of ^{111}In in Ag are similar to those observed after the implantation of ^{111}In into Ag_2O. We therefore suggest the placement of ^{111}In in an Ag_2O structure. Oxidation at higher temperatures[28] or disintegration of Ag_2O leads to a structure similar to that of In_2O_3. Just as expected in Ag, the transition from the metal oxide host to In_2O_3 precipitations can be observed at temperatures where the free energy is positive (e.g., at $T_{ox} > 500$ K).

2. Gold, platinum, palladium

The hyperfine parameters for the oxidation of ^{111}In in Au, Pt, and Pd (see Table I) also seem to indicate precipitation of In_2O_3. In the case of Au, already very low In concentrations (ppm level) result in an external oxidation of In.[29] The large differences among the samples may be caused by surface effects. Oxygen is also nearly insoluble in Pt and external oxidation is expected, but the present data do not exclude internal oxidation.

D. Conclusions

The present investigation of the oxidation of ^{111}In after implantation into fcc metals clearly illustrates the virtues and limitations of the PAC technique to probe chemical reactions in solids on the atomic level. In the absence of nearby radiation-induced defects, substitutional ^{111}In atoms experience no quadrupole hyperfine perturbation in a cubic bulk. This situation changes as soon as ^{111}In is starting to trap oxygen and to form ^{111}In-O_x complexes. We like to emphasize that in the present experiments some 10^{11} oxidized probe atoms can be easily detected. As illustrated in Fig. 5, this trapping mechanism sets in at about half the melting temperature of the host.

A second conclusion is that in most cases the ^{111}In-O$_x$ structure essentially determines the EFG parameters and not the lattice constant of the bulk. This can be directly inferred from the similarity of the PAC patterns in the different hosts studied, as shown in Fig. 6.

An obvious limitation of the PAC technique comes from the fact that the observed frequency distributions are rather broad, leading to strongly damped PAC spectra (see Fig. 6). For this reason, possible details of the structures of the ^{111}In-O$_x$ complexes cannot be resolved, like the number of ^{111}In atoms in each complex, the number of oxygen ions, the size of the precipitates, and so on.

In this somewhat disappointing situation, the investigation of PAC spectra of ^{111}In implanted into some metal oxides was of great importance: First, we observed complexes with well-defined EFG parameters, which we interpret as substitutional ^{111}In ions in the metal oxide. This interpretation is based on the observed Larmor precession typical for ^{111}In in antiferromagnetic NiO and on the deduced asymmetry parameters η which agree with the respective predictions of the point-charge model. Second, we identified in AgO and Ag$_2$O fractions with broadly distributed quadrupole frequencies (like in the metals) centered at the same main frequencies $\langle\omega_1\rangle$ as the well-defined complexes. That means that all ^{111}In sense a similar EFG, but that often the ionic sites vary slightly. This (small) variation of the In—O bond length will be discussed below. This observation and the very precise determination of the PAC parameters for ^{111}In in In$_2$O$_3$ allowed us to identify the general ^{111}In-O$_x$ complex observed after the oxidation process as In$_2$O$_3$, but with broadly distributed PAC parameters. Most probably, In$_2$O$_3$ precipitates are formed in agreement with the free-energy argument. This is the explanation for the similarity of the oxidation processes observed in this series of experiments. The influence of the host metal is only weak if there is any. Further PAC and electron-microscopy experiments are presently carried out to estimate the size of these precipitates.

Some explanations for broadly distributed EFG parameters have been discussed in Sec. II. An obvious explanation put forward by several authors is the presence of nearby radiation defects. However, in the case of the metal hosts and In$_2$O$_3$ all defects had been annealed out. In addition, we have seen very little damping of the PAC spectra taken directly after ^{111}In implantation in NiO. We thus favor a different explanation of the observed broad frequency distributions previously proposed by Bolse et al.[8] The point-charge model for ^{111}In on substitutional sites in In$_2$O$_3$, AgO, and Ag$_2$O makes predictions of the quadrupole frequency ν_Q^p and the asymmetry parameter η^p which can be compared with the experimental figures ν_Q^{expt} and η^{expt}. Defining the ratio $\beta=\nu_Q^{\text{expt}}/\nu_Q^p$ as the "antishielding" factor, it turned out that β is a very sensitive function of the In—O bond length. When changing the bond length by as little as 0.2 Å, β sharply increases from 3 to 40, e.g., by more than a factor of 10. This happens at a distance between oxygen and ^{111}In which corresponds to the sum of the ionic radii $r(\text{In}^{3+})$ and $r(\text{O}^{2-})$. In this critical range, the typically 40% width of the frequency distribution can be traced to a variation of only 0.05 Å in the In—O bond length. Such small displacements caused by the mismatch between the InO$_x$ structure and the actual host are hard to detect by any other method and this observation may well offer new applications of the PAC technique if the calibration of the EFG has been established in more cases.

ACKNOWLEDGMENTS

[1]R. A. Rapp, Corrosion 21, 382 (1965).

[2]C. Wagner, Z. Elecktrochem. 63, 772 (1959).

[3]A. F. Pasquevich, A. G. Bibiloni, C. P. Massolo, F. H. Sanchez, and A. Lopez-Garcia, Phys. Lett. 82A, 34 (1981).

[4]P. Wodniecki and B. Wodniecka, Hyperfine Interact. 12, 95 (1982).

[5]W. Bolse, H. Schröder, P. Wodniecki, M. Uhrmacher, and K. P. Lieb, Phys. Lett. 93A, 429 (1983).

[6]H. Schröder, W. Bolse, M. Uhrmacher, P. Wodniecki, and K. P. Lieb, Z. Phys. B 65, 193 (1986).

[7]W. Bolse, M. Uhrmacher, and K. P. Lieb, Mater. Sci. Eng. 69, 375 (1985).

[8]W. Bolse, M. Uhrmacher, and J. Kesten, Hyperfine Interact. (to be published).

[9]E. Recknagel and Th. Wichert, Nucl. Instrum. Methods 182/183, 439 (1981).

[10]F. Pleiter and C. Hohenemser, Phys. Rev. B 25, 106 (1982).

[11]Th. Wichert, Hyperfine Interact. 15/16, 335 (1983).

[12]The Electromagnetic Interaction in Nuclear Spectroscopy, edited by W. D. Hamilton (North-Holland, Amsterdam, 1975).

[13]F. Faether (unpublished).

[14]A. R. Arends, C. Hohenemser, F. Pleiter, H. de Waard, L. Chow, and R. M. Suter, Hyperfine Interact. 8, 191 (1980).

[15]J. Kajfosz, Institute of Nuclear Physics (Cracow), Report No. 858/PM, 1973 (unpublished).

[16]J. D. Rogers and A. Vasquez, Nucl. Instrum. Methods 130, 539 (1975).

[17]M. Forker, L. Freise, and D. Simon, Z. Naturforsch. 41a, 403 (1986).

[18]A. G. Bibiloni, J. Desimoni, G. P Massolo, L. Mendoza-Zelis, A. F. Pasquevich, F. H. Sanchez, and A. Lopez-Garcia, Phys. Rev. B 29, 1109 (1984).

[19]A. Abragam and R. V. Pound, Phys. Rev. 92, 943 (1954).

[20]M. Forker, Nucl. Instrum. Methods 106, 121 (1973).

[21]F. James and M. Roos, CERN Computer Centre, Program Library D506/D516, 1977 (unpublished).

[22]M. Uhrmacher, K. Pampus, F. J. Bergmeister, D. Purschke, and K. P. Lieb, Nucl. Instrum. Methods B **9**, 234 (1985).

[23]High Voltage Engineering Europa, Heavy Ion Source Model S055, Brochure HVEE 25980 (unpublished).

[24]See J. P. Biersack and J. F. Ziegler, in *Ion Implantation Techniques*, edited by H. Ryssell and H. Glawischnig (Springer, Berlin, 1982), p. 122. for a discussion of the DIMUS routine.

[25]Z. Ovadyahu, B. Ovryn, and H. W. Kraner, J. Electrochem. Soc. **130**, 917 (1983).

[26]A. F. Pasquevich, F. H. Sanchez, A. G. Bibiloni, J. Desimoni, and A. Lopez-Garcia, Phys. Rev. B **27**, 863 (1983).

[27]A. Bartos (private communication).

[28]J. Kesten, P. Wodniecki, M. Uhrmacher, and K. P. Lieb (unpublished).

[29]A. F. Pasquevich, A. Hoffmann, R. Vianden, and U. Wrede, J. Appl. Phys. **58**, 3200 (1985).

[30]C. Hohenemser, A. R. Arends, H. de Waard, H. G. Devare, F. Pleiter, and S. A. Drentje, Hyperfine Interact. **3**, 297 (1977).

[31]R. W. G. Wyckoff, *Crystal Structures* (Interscience, New York, 1963).

[32]H. T. Spath, H. G. Winkler, and K. Tovkar, *Reactivity of Solids* (Chapman and Hall, London, 1972), p. 745.

[33]J. Kesten, dipoloma thesis, Universty of Göttingen, 1984 (unpublished).

[34]H. H. Rinneberg and D. A. Shirley, Phys. Rev. B **13**, 2138 (1976).

[35]M. Marezio, Acta Crystallogr. **20**, 723 (1966).

[36]M. Uhrmacher and W. Bolse, Hyperfine Interact. **15/16**, 445 (1983).

[37]C. Wagner, Z. Elektrochem. **63**, 772 (1959).

[38]A. Atkinson, Rev. Mod. Phys. **57**, 437 (1985).

[39]K. Hauffe and P. Kofstad, Z. Elektrochem. **59**, 339 (1955).

[40]H. Jehn, W. Hehn, E. Fromm, and G. Hörz, in *Gases and Carbon in Metals*, edited by H. Behrens and G. Ebel (Fachinformationszengrum Energie, Physik, Mathematik GmbH, Eggenstein-Leopoldshafen, 1982), Vol. XXII.